Study of Biofilm Formation of the *Samonella Enteritidis* in 3D Bioprinted Constructs

Madeleine Monperrus
madeleine@monperrus.net

under the direction of
Dr. Siva Koti Sangabathuni
AIMES

Research Academy for Young Scientists
July 13, 2022

Abstract

It is estimated that 65 to 80 percent of the human infectious are cause by biofilms according to the National Institutes of Health and the Center for Disease and Prevention. Therefore, bacterial biofilms are serious global health concern and the study of biofilm formation is primordial to be able to locate and fight bacteria more efficiently. This article studies biofilm formation of *salmonella enteritidis* by observing the development of amyloid fiber-forming protein curli and polysaccharide cellulose using optotracers. By cultivating and growing S. enteritidis and calcofluor, supplemented agar plates, we monitor the synthesis of biofilm through a fluorescence spectrophotometer. This enables the observationf of biofilm of S. Enteritidis. This paper also investigates the diameters of triangular constructs printed at various speeds and pressure. Pressure is found to have a greater impact on the thickness of the printed construct than speed and should therefore be changed carefully. It is concluded that is that both speed and pressure are important factors in the printing of 3D constructs as wrong values could result in potentially unsuccessful extrusion. By developing G-code and printing letters with hydrogel supplemented with rhodamine dye a conclusion was that the potential replacement of rhodamine with the salmonella could mimic 3D micro environment of the body to betetr understand biofilm formation.

Acknowledgements

I would like to express my immense gratitude towards my mentor Doctor Siva Koti Sangabathuni for the enormous support provided, the laughs and the time spent in teaching me as much as possible in only two weeks. Thank you to the Senior Lab Manager Elham Jalalvand for showing me the right way to act in a BSL2 corridor and meaning full discussions about manga and neuroscience. Thank you to Linda Thörn for the help and kindness. I would like to acknowledge the insight full feedback given by Professor Ferdinand X. Choong and Agneta Richter-Dahlfors. Thank you to you both.

Without Rays- for excellence, this paper wouldn't exist so a whole bucket of thankfulness to this years' organizers for being there and fixing everything after only (very) few hours of sleep. Thank you to Ann-Kristin Malz, Julia Mårtensson and Miranda Carlsson. Thank you to all the xRays as well for the harsh (sometimes) but needed feedback. Thank you to Julia Jansson, Shirley Lidman, Kelvin Szolnoky, Serhat Aktay. Thank you to my dad for reading my paper and giving me the envy to dive deeper into the world of research.

Finally, thank you to Rays' collaborative partners Bejerstiftelsen and Kungliga Patriotiska Sällskapet for making this whole experience possible.

Contents

1 Introduction

Biofilm formation can be studied using optotracers and fluorescent microscopes. For more accurate resuts, 3D bio-printing should be used to observe biofilm formation of bacteria in three dimensional constructs.

1.1 Background

In natural environments, most bacteria as well as microorganisms live in a biofilm culture [1]. Biofilm formation designates a particularity of bacteria and microbes to aggregate, adhere to a surface and synthesise an extra cellular matrix (ECM) [2, 3, 4]. The ECM is the case of bacterial biofilm is a complex network of proteins, polyssaccharides and other molecules which surrounds and supports the bacteria community. The ECM in which they are embedded protects from outside threats thus ensuring higher survival changes and increasing colonization rate [3].

Previous studies studying bacterial biofilm formation oversee the heterogeneity of biomass. The diversity of bacteria and spatial complexity of a single biofilm has been overlooked. This has become a main problem in the study of bacterial conglomerates and their biofilm formation [5].

The widespread method for biofilm studies utilizing agar culture, a widespread method for cultivating micro organisms. The conditions in which the bacteria is studied has however several drawbacks affecting the reproducibility of the results to determine microbial inhibition concentration [5]. Other methods include the use of modelling with flow chambers or bioreactors. However, bioreactors are unsatisfactory due to the main drawbacks being the limited number of individual strains which can be analyze simultaneously and the high risk for contamination due to the design of the reactors [5]. Flow chambers systems is limited by the the high cost of the equipment and methodological complexity. All three aforementioned methods share the common problem of the high variability of the obtained biofilms parameters and reproducibility of the results [5].

A new proposed method is 3D bio-printing, a field which is currently one of the emerging growing areas of engineering [5, 6]. 3D bioprinting is employed to generate 3D models, which mimic 3D microenvironment of the human body. While traditionally used for research and regenerative medicine and tissue engineering, bacteria cells have started being used instead of mammalian and plants cells for research [5].

Bacteria studied in three-dimensional hydrogel constructs have demonstrated increased metabolic activity, antimicrobial resistance, and plasmid stability compared to 2D biofilm models potentially indicating the 3D models to be more closely mimicking natural bacterial growth in vivo when compared to classic 2D models and methods [7].

A number of atoms and molecules have the property to absorb light at a certain wavelength and re-emit light at a longer wavelength after a brief interval. When the atom absorbs energy, electrons jump from ground state to excited state. After certain internal, these electrons return to their ground state by releasing energy. The phenomena of releasing of energy from lowest excited state to ground state termed as fluorescence (Figure 1).

Fluorescent microscopy, unlike conventional light microscopes are able to emit and capture a wider variety of wavelength. The simple principles behind the functioning of molecular spectroscopy which encompasses fluorescent microscopy can be explained by Jablonski diagrams. Figure 1a, representing a Jablonski diagram displays a visual depiction of the way fluorescence works. Electrons are excited by photons with a specific wavelength which results in moving them into higher energy levels. When falling back to the ground state, these electrons release energy in the form of photons and thus emit light [8]. Figure 1b shows the excitation peak required for a molecule to move the electron from ground states to higher energy levels and emission peak when electrons return to ground state, respectively. Emission peak always appear at longer wavelength compare to absorption or excitation peak [9]. When using known and researched fluorescent molecules for fluorescence spectroscopy, both wavelengths are already pre defined and set by the instruments. Otherwise, the right excitation peak wavelength and emission wavelength are

determined by UV absorption spectroscopy and fluorescence spectroscopy. Fluorescence and has many advantages which enables to detect, trace and observe molecules.

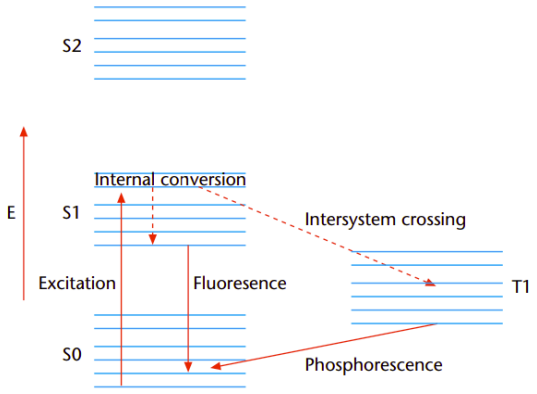

(a) Depicts the principles of a Jablonski diagram where electrons are excited from one state to a higher energy state during excitation and emit light during emission. Displays electrons jumping from higher singlet to a lower singlet in the process called fluorescence as well as when electrons travel from a higher singlet to a lower triplet and back to ground state, a process named phosphorescence. [10]

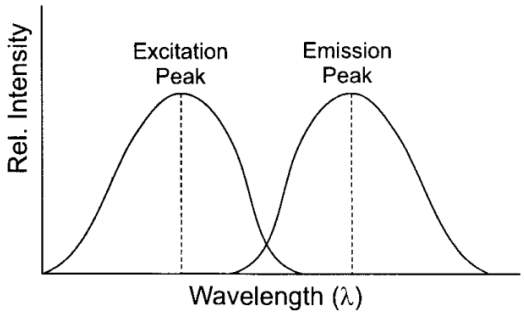

(b) Wavelength for both the excitation peak (when an electron gets excited from a lower to a higher energy level) and the emission peak (when the electron falls back from a higher to the energy level it got excited from. The figures shows that the excitation peak is usually emitted at lower wavelength in comparaison to the emission peak[9]

Figure 1: Explains the fundamentals of fluorescence through a Jablonski diagram and graph display the aproximatly the placement of the excitation and emission peaks on the electromagnetic spectrum.

Recently, optotracers such as Ebbabiolight 680 has been discovered and used to detect and monitor the curli formation during biofilm formation of the salmonella enteritidis. They are used in this paper as tracing methods to monitor biofilm formation. The use of fluorescence in the detection and tracing of certain molecules has been improved over the years [9]. Recent discoveries enable the tracing of targeted fluorescent molecules that are incorporated in DNA green fluorescence proteins (GFP) including optotracers. Optotracers are fluorescent molecules which bind targeted molecules via electrostatic interactions [4]. Optotracers are currently used to target and enable the tracing of amyloids. This is done by spectral discrimination of amyloid morphotype. When optotracers bind with the amyloids will lead to a shift in fluorescence excitation and an increase in fluores-

cence emission intensity which in turns enables the real-time detecting and tracing of the targeted molecules[4].

1.2 Biofilm formation

Biofilm formation is a form of growth used by microorganisms. The term biofilm describes the complex structure when microorganism agglomerate and produce a protective layer around themselves [8]. This report focuses on formation of the biofilm by salmonella enteritidis.

Unlike a planktonic form of bacterial culture where single cells float in free-weighted state, biofilms consist of large collections of adherent populations of bacteria surrounded by an extra cellular matrix (ECM) [5] and are attached to a biotic surfaces or abiotic surface [11]. Bacterial biofilm is a form of protection against foreign causes of stress or danger such as antibodies, phagocytes and antibiotics in host tissues, or inhospitable conditions (UV lights, heat, cold, shear forces ect.) on inert hostile surfaces [12].

The ECM is produced by the bacteria itself and is composed by various polymers such as exopolysaccharides (EPS), nucleic acids (eDNA and eRNA [1]), proteins, lipids, and other biomolecules [13]. Although the components of this matrix varies from species to species, some elements such as adhesins, amyloid proteins and polysaccharides are considered ubiquitous [14, 2]. For the *Salmonella Entiritidis* bacteria, two main ECM components can be identified; the amyloid curli protein and the polysaccharide cellulose [3].

The formation of biofilm is dependent on multiple factors, such as temperature and quality of growth medium [11]. Approximately 99% of all bacteria are believed to exist naturally in biofilm formation, 65-80% of which are estimated to be the cause of human infections [11, 1, 5].

The biofilm community behaviour provides an increase in protection against several external threats such as antibiotics, host immune systems, and other environmental factors leading to greater colonization [3, 15, 11, 16]. Above all, the ECM in which the pop-

ulations are encased provides shielding against antagonistic environments [12]. Disease causing bacteria in biofilm are harder to detect using simple clinical detection methods in comparison to planktonic bacterial growth due to the extra cellular method and adhesion of the populations on the host tissues [12]. Human infections caused by such bacteria are therefore detected later than disease caused by bacteria not forming biofilm.

The amyloid curli protein, one of the two major components of the S. entriditis biofilm is also believed to be involved in numerous neurocognitive related diseases, such as Alzheimers, Huntingtons and Parkinsons' diseases [17].

1.3 3D-Bioprinting

A shortage of studies studying the formation and growth of bacteria in 3D leads to inaccurate observations of bacteria proliferation. Traditional observations of bacteria occur only in two dimensional space, usually on well plates or petri dishes [5]. This does not accurately represent the real life growth of bacteria as the environment of the body offers a three dimensional space to proliferate in[5].

Using additive manufacturing techniques and bio inks, three dimensional constructs can be printed and used to study cells in a more natural environment[5].

Different 3D bio-printers are currently available on the market. Mainly three different methods to print are used for research, inkjet extrusion, pressure based extrusion and laser[6]. Pressure based extrusion bio-printer is the most commonly used due to its effectiveness and design. Extrusion-based bio-printing was rapidly developed over the years to enable simpler and cheaper bio-printers. Two main principles are currently in use: pneumatic- and mechanical-driven fluid dispensing system[18]. The principles of pneumatic extrusion are displayed in Figure 2. During pneumatic extrusion, air pushing the bio ink out of a syringe through a nozzle [18]. Following the extrusion of the bio ink out of the nozzle, the material is being deposited on a surface which traditionally may be an agar plate, glass slide or well plates [18]. The whole syringe is able to move in the x-, y- and z-directions to form shapes. Constructs may also be printed in fluids [18]. The

pressure at which the air is pushed as well as the speed at which the syringe moves can be controlled throughout the printing.

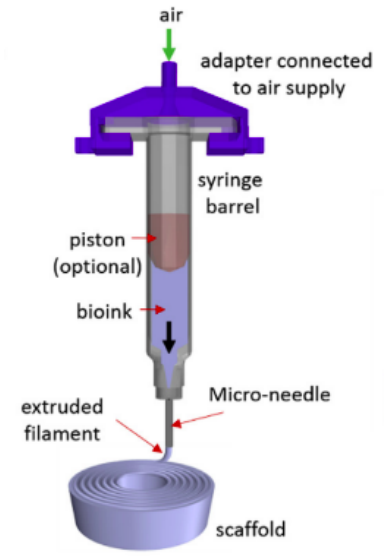

Figure 2: **Annotated diagram of a pneumatic syringe used in extrusion based 3D bio-printing.** Air is pushed through an adapter which connects to the syringe. The bio ink is in turn pushed out of the syringe through the nozzle which extrudes the material on a chosen surface. The syringe is able to move in x-, y- and z-coordinates [19].

The advantages of extrusion based would be the printability of highly viscous, high cell densities bio ink. This is useful when printing material which needs those properties to print a successful construct. The applicability of multimaterial bio-printing and comparatively simple bio-printing process are more advantages [18]. The disadvantages would be the relatively slow printing speed, low to medium resolution highly dependent on setup and the moderate cell viability $(40 - 80\%)$ dependent on setup. extrusion based bio-printers are also able to continuously extrude material without interruption.

Successful bio-printing requires the right bio ink choice. Factors such as bio-compatibility, viscosity and cell density determine microenvironment of target. Printability describes the ability of a bio ink to result in successful constructs after printing.

2 Method

This method was divided into two main experiments. The first experiment investigates biofilm formation of S. Enteritidis when cultivated at 28° for four days. The second one includes 3D bio-printing of triangular shapes at different speeds and pressure to examine the importance choosing at what pressure and speed to print.

2.1 Experiment A: Investigation of Bacterial Biofilm

Colonies of bacteria were cultivated and incubated for four days. The resulting biofilm was imaged using fluorescent microscopy at day 1 and day 4 after the start of the incubation.

2.1.1 Materials

BIO X6 cellink bioprinter was used to print 3D constructs. Blue color (20G) 410 µm nozzle and testing ink was purchased from Cellink company, Sweden. Ebbabiolight 680 was ordered from Ebba Biotech AB, Sweden. Luria Broth Agar powder and calcofluor was ordered form sigma Aldrich and used as they received. BioTek Lionheart FX automated microscope was used to take fluorescence image of the samples. The whole sample was scanned with 1.25X magnification with 7 by 5 tiles. Image tiles were stitched and processed to get final images. For 3D printed samples, 12 by 12 tiles with 1.25X magnification was used.

2.1.2 Preparation

The S. Enteritidis strains 204 and 207 were used during the experiment. S. Enteritidis wild-type strain 3934 (wt), named strain 204 is Gram positive and was used as a positive control as it is able to synthesise both curli protein and cellulose. The Gram negative S. Enteritidis, the isogenic mutants $\vec{\Delta}$csgD, labelled 207 strain however, since lacking the production of both cellulose and curli, was used as the negative control of the experiment. Both strains had previously been transformed and genetically modified to enable green

fluorescent protein (GFP) expression.

The media used to culture and dilute the bacteria colony was lysogeny broth (LB) without salt. The petri dishes filling was LB agar. The preparation of LB contained 10g of triptone, 5g of yeast extract, 15g of agar and 1L of MiliQ autoclaved water. For preparing fluorescent LBA plates, 5 ml of LBA containing EbbaBiolight 680 (2 µl/ 5 ml of LBA) and calcofluor (5 µl/ 5 ml of LBA) casted on 60 mm petridish to make printed bed level uniform.

Bacteria were routinely cultured on lysogeny broth (LB) (w/o) salt in an incubator at 37°. One colony was selected and inoculated in lB agar media then placed in a shaking incubator at 28° overnight. The exponentially grown bacteria was then diluted with 100mL of sample mixed with 100mL of LB media. A spectrophotometer was used to measure the absorption of the four different samples. These measurements were then used to calculate the concentration of bacteria in each sample. The absorption of the ARD 204A was 1.4 which has $7 - 8x10^8 CFU/$mL and ARD 207A was 1.2, which has $7 - 8x10^8 CFU/$mL.

2µL drops of each sample were used as inocula on four agar plates containing optotracers EbbaBiolight 680 and Calcofluor as indicated above. The samples were incubated at 28° for approximately four days. Fluorescent imaging of cells and ECM was conducted one and four days after the start of the incubation using a Lionheart™ FX Automated Microscope (Ramcon, Sweden).

For fluorescence imaging of the biofilm formed, the below parameters and filters are used. Lionheart is used to image Biofilm formation with 1,25X magnification, with 7 by 5 tiles of biofilm area. For imaging Ebba 680: PI filter is used (Excitation: 530-565 nm, Emission: 600-800 nm). For Calcofluor: DAPI filer is used (Excitation: 337 nm, Emission: 477 nm). For GFP: GFP filer is used (Excitation: 475 nm, Emission: 509 nm)

2.2 Experiment B: 3D bio-printing

The 3D-bioprinter model used was BioX[6] from the CELLINK company. Hydrogel from the same company was used for all the experiments. Three 6cm petri dishes were used to

print. Triangles of the size 10mm X 0.6 mm were printed on two petri dishes while four different shapes were printed on the last one. All shapes were printed using a 100mm L syringe with a nozzle of diameter 410µm. The pressure and speed of the printhead was varied for the different constricts according to Table 1. All printed constructs were imaged with a Lionheart™ FX Automated Microscope (Ramcon, Sweden) in order to measure the diameter of the constructs with higher accuracy. The experiment was performed in triplicates. The whole printing process was repeated three times for each individual petri dish and a mean was taken between the shapes to determine at what level of accuracy the shapes were printed at.

The G-code was developed and hydrogel containing the fluorescent molecule rhodamine for printing the letter AIMES and RAYS on a 10cm petri dish. Rhodamine can be used for fluorescent microscopy. A smiley face was also printed using the same bio ink. Both constructs were then imaged using a Lionheart™ FX Automated Microscope (Ramcon, Sweden) and processed to see the constructs appear as fluorescent.

Table 1: The speed and pressure at which different figures were printed.

petri dish	figure	speed (mms^{-1})	pressure (kPa)	shape
1	1	10	15	triangle
	2	10	20	triangle
	3	10	25	triangle
	4	10	30	triangle
2	1	10	25	triangle
	2	15	25	triangle
	3	20	25	triangle
	4	30	25	triangle
3	1	10	25	honeycomb circle
	2	10	25	square
	3	10	25	pyramid
	4	10	25	star

3 Results

Photographs of the biofilm of strains 204 and 207 for both day 1 and day 4 are grouped into two figures. The architecture of the ECM is visible. The 3D printed constructs have been imaged and displayed in figures as well.

3.1 Experiment A: Investigation of Bacterial Biofilm

Biofilm forms outwards with curli and cellulose both distally projecting radial patterns. Figure 3 shows an increase in bacteria formation for the undiluted strains 204 A and 207 A. This may be due to the dilution of the bacteria in samples 204 B and 207 B. No

synthesis of curli nor cellulose can be observed day 1.

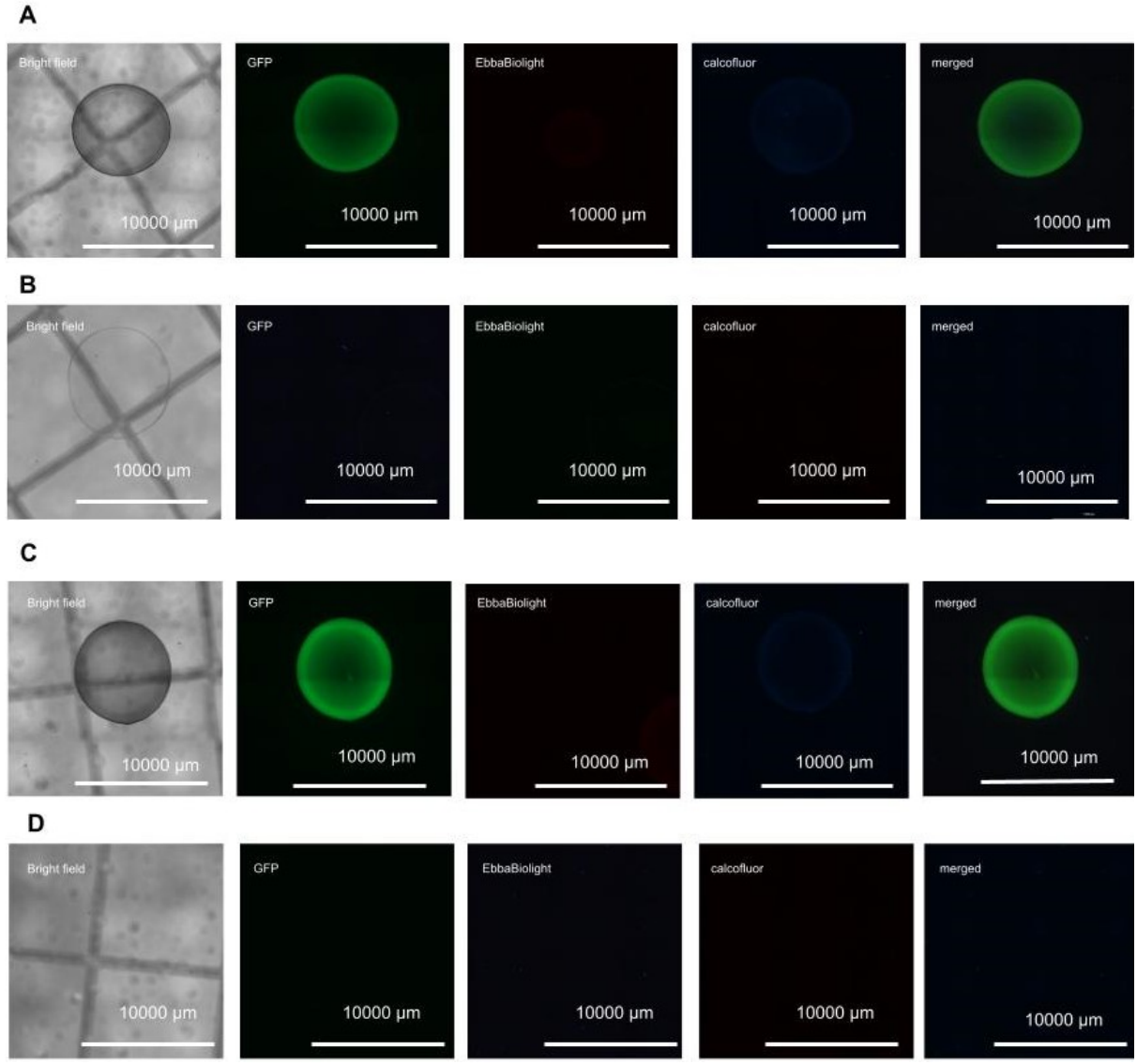

Figure 3: **Imaging of biofilm on a 4 agar plates at day 1.** Biofilm formation day 1 after growth of bacteria on agar supplemented with Ebba680 and calcofluor. Morphology of the bacteria is shown in brightfield for **(A)** strain 204 (undiluted, curli+, cellulose+), **(B)** 204 (diluted, curli+, cellulose+), **(C)** strain 207 A (undiluted, curli-, cellulose-), **(D)** strain 207 B (diluted, curli-, cellulose-). Spatial distribution of the bacteria is shown through fluorescence microscopy with GFP (green), ECM curli (Ebba680 in red) and ECM cellulose (calcofluor in blue). Images are visualized separately and merged for each respective strain. Scale bar = 10000µm.

Formation of channels may be observed at day 4 (see Figure 4) with development of both curli and cellulose reaching towards the outside. The architecture of the ECM is especially visible with the images of 204 B (D) in figure 4. No bacteria, curli or cellulose are

present in 207 B (figure 4, (D)). The synthesis of channels and radial patterns indicate an organized ECM while the lack of curli and cellulose at day 1 shows that the development of ECM occurs at ater stages of biofilm formation.

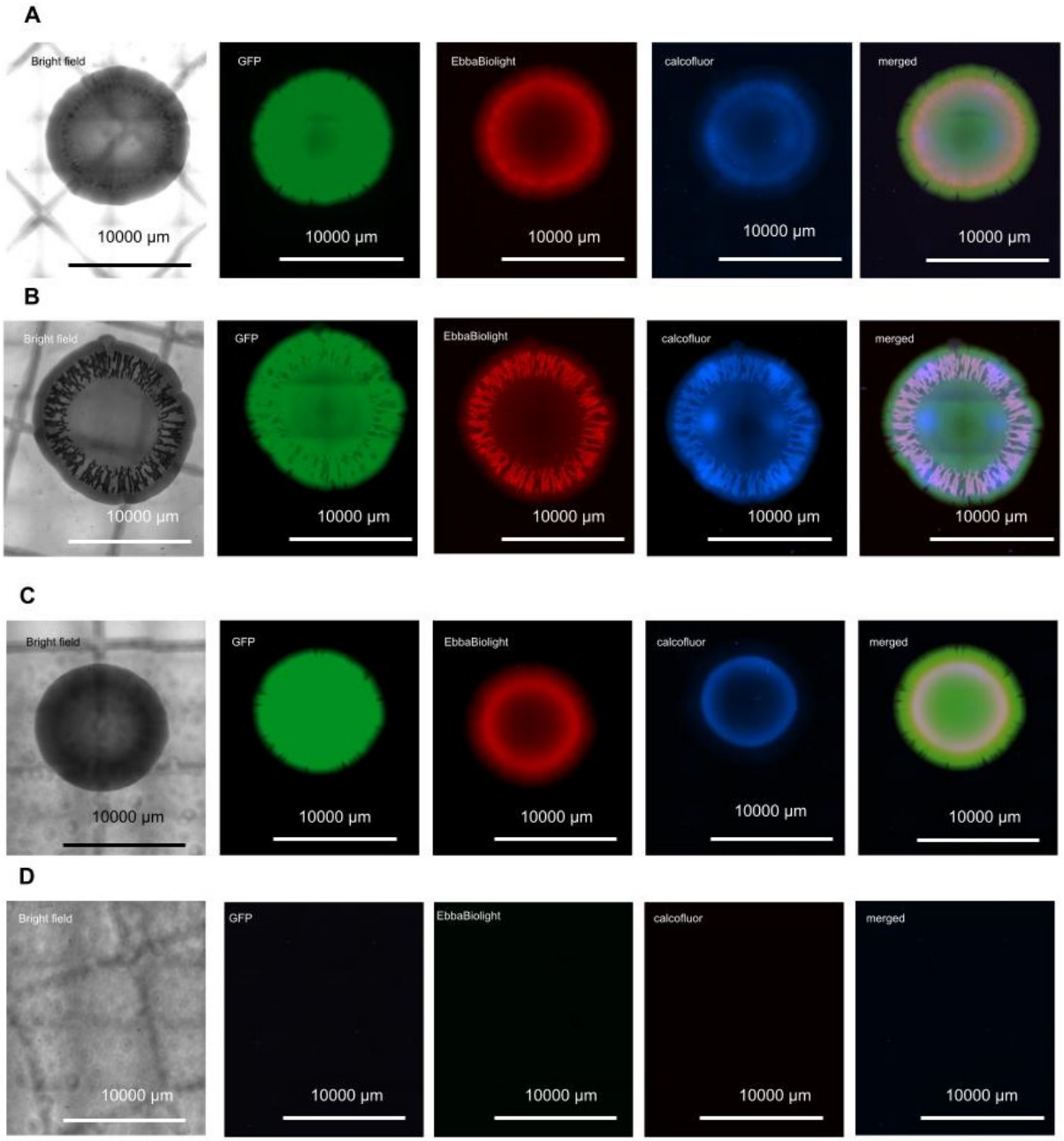

Figure 4: **Imaging of biofilm on a 4 agar plates at day 4.** Biofilm formation day 1 after growth of bacteria on agar supplemented with Ebba680 and calcofluor. Morphology of the bacteria is shown in brightfield for **(A)** strain 204 (undiluted, curli +, cellulose +), **(B)** 204 (diluted, curli+, cellulose+), **(C)** strain 207 A (undiluted, curli-, cellulose-), **(D)** strain 207 B (diluted, curli-, cellulose-). Spatial distribution of the bacteria is shown through fluorescence microscopy with GFP (green), ECM curli (Ebba680 in red) and ECM cellulose (calcofluor in blue). Images are visualized separately and merged for each respective strain. Scale bar = 10000µm.

3.2 Experiment B: 3D bio-printing

3.2.1 Pressure

Change in pressure affects thickness diameter with high correlation ($\beta = 25.7427; [19.106 - 32.379]; P < 10^{-3}$).). Change in thickness is observed when the same construct is being printed with different pressures and consistent speed (Figure 5). Unsucessful extrusion is also noticed in shape 1, figure 5.

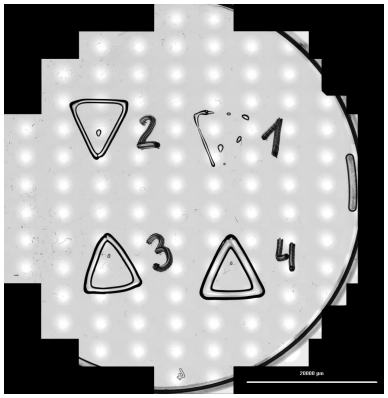

Figure 5: **Automated microscopy imaging of 4 printed constructs.** Photograph of triangular shapes printed at various pressure and constant speed. With pressures of 15 kPa **(1)**, 20 kPa **(2)**, 25 kPa **(3)** and 30 kPa **(4)**(see Table 1). The speed is kept constant at 10^{-1}. Unsuccessful extrusion is observed in **(1)**. Printed with nozzle diameter of 410µm. Scale bar = 10000µm.

An increase in thickness occurs with an increased pressure for the same construct when printed with constant speed (Figure 6).

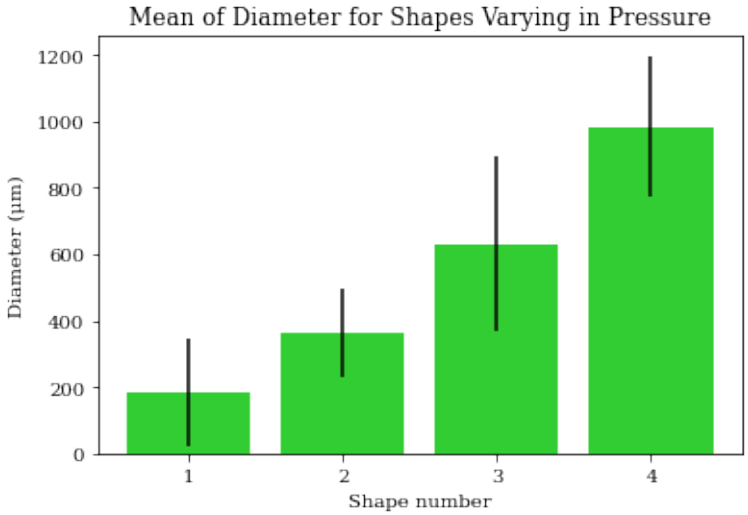

Figure 6: Change in diameter of constructs' sides in relation to change in pressure. The mean between three similar shapes is calculated and displayed for the side diameter of shapes **(1, 2, 3 and 4)**. Standard deviations are added for each individual shape.

3.2.2 Speed

Change in speed affects thickness diameter according to $\beta = 23.6573; [8.304 - 39.011]; P = 0.006$) is observable. A decrease in diameter of the printed construct in relation to the increase of speed is observable.

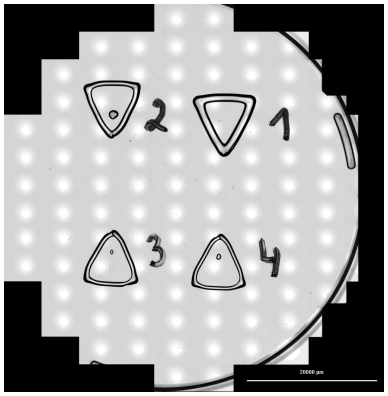

Figure 7: **Automated microscopy imaging of 4 printed constructs.** Photograph of triangular shapes printed at various speed and constant pressure. With speeds of 10 mm^{-1} **(1)**, 15 mm^{-1} **(2)**, 20 mm^{-1} **(3)** and 30 mm^{-1} **(4)** (see Table 1). The pressure is kept constant at 25 kPa. Printed with nozzle diameter of 410µm. Scale bar = 10000µm.

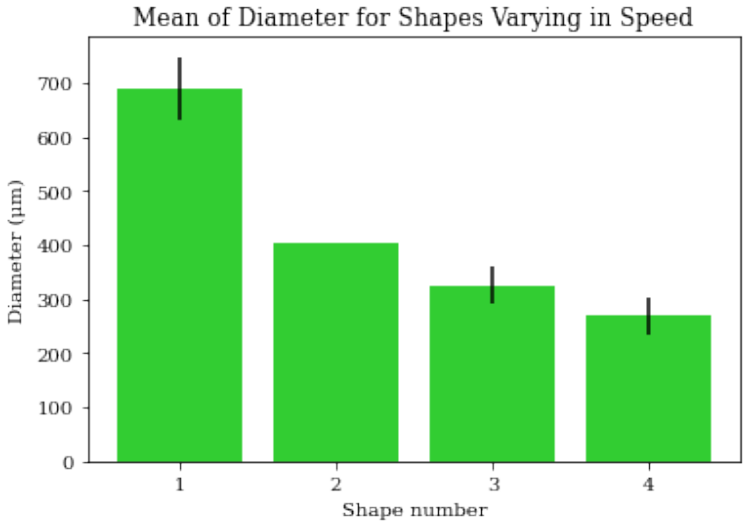

Figure 8: Change in diameter of constructs' sides in relation to change in speed. The mean between three similar shapes is calculated and displayed for the side diameter of shapes **(1, 2, 3 and 4)**. Standard deviations are added for each individual shape.

3.2.3 Shapes

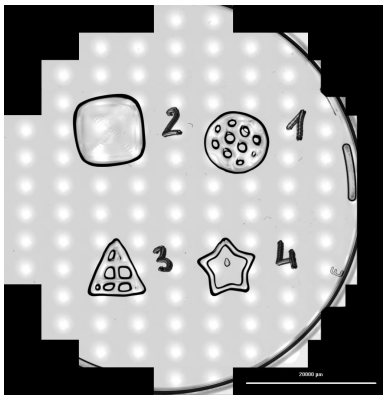

Figure 9: Automated microscopy imaging of 4 printed constructs. Photograph of various shapes printed at constant speed and constant pressure. With speed of 10 mm^{-1} and pressure of 25 kPa kept constant for all four constructs. All constructs were printed using G-code existing in the CELLINK software. A circle **(1)** with honeycomb filling size 10mm in diameter and 0.6mm height and filled by 25% , square **(2)** with size 10mm x 10mm and height 0.6mm filled by 99.99% with concentric squares, triangle **(3)** with dimensions of 10mm x 10mm x 0.6mm and filled with windowfilling by 25% and a star **(4)** with dimensions 10mm x 0.6mm. Printed with nozzle diameter of 410µm. Scale bar = 10000µm.

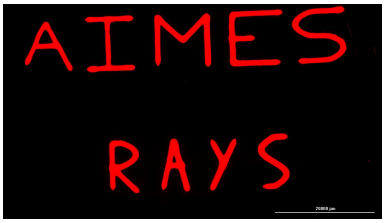

Figure 10: Fluorescent microscopy of printed letters AIMES and RAYS with rhodamine supplment (appearing in red). G-code was developed manually (see Appendix for complete G-code). Printed with nozzle diameter of 410µm. Scale bar = 10000µm.

4 Discussion

Regarding the biofilm experiment, results demonstrate the expression of curli protein and cellulose at day 4. The resulting formation of biofilm is organized in radial patterns around the original drop of bacterial media. Expression of both curli and cellulose are observed in strains 204 A, 204 B as well as 207 A. Table **??** (D), representing 207 B shows no trace of bacteria nor biofilm formation. This may be seen by the lack of emission from the GFP molecule. A total lack of bacteria for the strain 207 B might be due to experimental error. The optotracers used enable the detection of the ECM architecture and the fluorescence microscopy revealed organized channels growing outwards for both curli protein and cellulose.

When looking at the results of the 3D bioprinted constructs, clear change in constructs thickness can be observed in figures 5 and 7. Moreover, the graphs 6 and 8 reveal a clear correlation between change in pressure or speed and change in thickness of the printed construct. In case of the change in pressure experiment, a positive correlation can be seen as the diameter of the printed sides of the triangular shape. An increase in thickness results in an increase in pressure. This correlation is significant as shown by the p-value calculated. When looking at the graph displaying the change in thickness in relation to the change in speed, one can see a negative correlation meaning that increasing speed results in decreasing diameter of the printed constructs. Once again, these results are of relevance as demonstrated by the p-value calculated.

Based on these outcomes, one can deduct that both pressure and speed play a major role in the successfulness of the printed construct. In the case of a triangle of dimensions 10X0.6mm printed with a nozzle of diameter 410µm, the maximized speed and pressure according to the results would be $25kPa$ and $10mms^{-1}$.

The values resulting from the calculated diameters of the sides of the triangle have not been able to be taken for a few shapes (e.g. figure 5 shapes (1)) due to unsuccessful excursion. This has been due to low pressure or to high speed. Thus, it is possible to say that both pressure and speed are of importance as wrong values regarding pressure and speed might result in unsuccessful printing or inaccurate constructs. Therefore, the results regarding the maximized speed and pressure for printing with a 410µmm nozzle are of importance as the choice of pressure and speed are a major factor determining the outcome construct.

Large standard deviations in graph 6in comparison to the standard deviations in the graph 8 show that change in pressure has a bigger impact on thickness of a construct compare to change in speed. Changes in speed will result in relatively similar results while changes in pressure will have significant effects on the resulting printed construct.

Additionally, different shapes such as honey comb, square, triangle and star were printed with optimized pressure and speed. Bright filed imaging showed a successful extrusion of material to print constructs at optimized conditions. Further, a fluorescence compound, rhodamine chloride (1 µg/ml) was incorporated in the testing ink to mimic the bacteria. Inoculating the actual bacteria was not possible due to the time. We have developed a G code to print the words AIMES and RAYS with fluorescent ink. Figure 10 displays the printed 3D constructs of AIMES and RAYS with optimized parameters. Fluorescence imaging of the printed constructs showed the uniform distribution of rhodamine as well as printability of the structures meaning the same construct could successfully be printed with inoculated living bacteria in the bio ink.

5 Conclusion

When growing on a LB agar plate, the s. entiriditis bacteria produces both curli protein and cellulose in radial patterns centered around the original bacteria colony and reaching outwards. Optotracers Ebbabiolight can detect and monitor the biofilm formation. Further 3D printer has been used to optimize the printing parametes for triangle shapes confirms that pressure and speed indeed effect the printing process. With the optimized parameters, different shapes honeycomb circle, square, triangle and star were printed. G-code was developed to print different shapes and testing the printability. Finally, we have prepared fluorescence ink with rhodamine to print smiley, AIMES and RAYS. Fluorescence image shows uniform distribution of rhodamine. We believe that replacement of bacteria with rhodamine could mimic 3D microenvironment to study real biofilm invivo. When 3D bio printing constructs, change in pressure must be done carefully while change in speed is reliable and can be done without to much impact on the resulting construct. The decision of the right speed and pressure is also primordial for a successful result as methods for bacterial detection are needed to advance the infection research and diagnostics.

Further studies will be required to study the biofilm formation of bacteria in 3D bio printed constructs to be able to draw conclusions on the growth of bacteria in three dimensional environments. Investigations of the possible usage of 3D bio printers in research regarding bacteria needs to be carried so that accurate descriptions of the growth of bacterial biofilm in natural environments can be found. Further studies may also investigate further the 3D print using bio ink with fluorescent bacteria to compare 2D evolution of biofilm with 3D evolution of biofilm.

References

[1] Ramos-Gallardo G. Chronic wounds in burn injury: a case report on importance of biofilms. World Journal of Plastic Surgery. 2016;5(2):175.

[2] Choong FX, Bäck M, Fahlén S, Johansson LB, Melican K, Rhen M, et al. Real-time optotracing of curli and cellulose in live Salmonella biofilms using luminescent oligothiophenes. npj Biofilms and Microbiomes. 2016;2(1):1-11.

[3] Choong FX, Huzell S, Rosenberg M, Eckert JA, Nagaraj M, Zhang T, et al. A semi high-throughput method for real-time monitoring of curli producing Salmonella biofilms on air-solid interfaces. Biofilm. 2021;3:100060.

[4] Butina K, Tomac A, Choong FX, Shirani H, Nilsson KPR, Löffler S, et al. Optotracing for selective fluorescence-based detection, visualization and quantification of live S. aureus in real-time. npj Biofilms and Microbiomes. 2020;6(1):1-12.

[5] Chapek S, Golovin S, Chikindas M, Ponomareva S, Rudoy D, Olshevskaya A. Application of 3D bioprinting in the study of bacterial biofilms. In: E3S Web of Conferences. vol. 273. EDP Sciences; 2021. p. 13010.

[6] Derakhshanfar S, Mbeleck R, Xu K, Zhang X, Zhong W, Xing M. 3D bioprinting for biomedical devices and tissue engineering: A review of recent trends and advances. Bioactive materials. 2018;3(2):144-56.

[7] Huang J, Liu S, Zhang C, Wang X, Pu J, Ba F, et al. Programmable and printable Bacillus subtilis biofilms as engineered living materials. Nature chemical biology. 2019;15(1):34-41.

[8] Donlan RM. Biofilms: microbial life on surfaces. Emerging infectious diseases. 2002;8(9):881.

[9] Herman B. Fluorescence microscopy. Garland Science; 2020.

[10] So PT, Dong CY. Fluorescence spectrophotometry. e LS. 2001.

[11] Eze EC, Chenia HY, El Zowalaty ME. Acinetobacter baumannii biofilms: effects of physicochemical factors, virulence, antibiotic resistance determinants, gene regulation, and future antimicrobial treatments. Infection and drug resistance. 2018;11:2277.

[12] Olson ME, Ceri H, Morck DW, Buret AG, Read RR. Biofilm bacteria: formation and comparative susceptibility to antibiotics. Canadian journal of veterinary research. 2002;66(2):86.

[13] Karygianni L, Ren Z, Koo H, Thurnheer T. Biofilm matrixome: extracellular components in structured microbial communities. Trends in Microbiology. 2020;28(8):668-81.

[14] Flemming HC, Wingender J. The biofilm matrix. Nature reviews microbiology. 2010;8(9):623-33.

[15] Gunn JS, Bakaletz LO, Wozniak DJ. What's on the outside matters: the role of the extracellular polymeric substance of Gram-negative biofilms in evading host immunity and as a target for therapeutic intervention. Journal of Biological Chemistry. 2016;291(24):12538-46.

[16] Sharma D, Misba L, Khan AU. Antibiotics versus biofilm: an emerging battleground in microbial communities. Antimicrobial Resistance & Infection Control. 2019;8(1):1-10.

[17] Tursi SA, Tükel Ç. Curli-containing enteric biofilms inside and out: matrix composition, immune recognition, and disease implications. Microbiology and Molecular Biology Reviews. 2018;82(4):e00028-18.

[18] Heinrich MA, Liu W, Jimenez A, Yang J, Akpek A, Liu X, et al. 3D bioprinting: from benches to translational applications. Small. 2019;15(23):1805510.

[19] Ozbolat IT, Hospodiuk M. Current advances and future perspectives in extrusion-based bioprinting. Biomaterials. 2016;76:321-43.

A Gcode

A.1 Triangle

```
; BEGIN_HEADER
; This file was generated by a biox6 from Circle 15x0,6mm.stl at 03.05.2022 10:51:27
; VERSION: 1.1.0
; PRINTER_NAME: biox6
; STL_FILE(S): Circle 15x0,6mm.stl
; DATE_TIME: 03.05.2022 10:51:27 Romance Daylight Time
; T1: TemperatureControlled
; END_HEADER
; generated by Slic3r 1.3.1-dev (Build (Unknown revision)) on 2022-05-03 at 10:51:27

; Print Config Notes:
; This profile prints tissue model with upright square lattice structure.
;
; external perimeters extrusion width = 0.45mm (1.49mm^3/s)
; perimeters extrusion width = 0.43mm (1.40mm^3/s)
; infill extrusion width = 0.43mm (1.40mm^3/s)
; solid infill extrusion width = 0.43mm (1.40mm^3/s)
; top infill extrusion width = 0.43mm (1.40mm^3/s)

M104 S200 ; set temperature
G28 ; home all axes
G1 Z5 F5000 ; lift nozzle

; Filament gcode
```

```
M109 S200 ; set temperature and wait for it to be reached
G21 ; set units to millimeters
G90 ; use absolute coordinates
M83 ; use relative distances for extrusion

;BIOX_ALTERNATING_PERIMETER_LAYER_0
G1 X0.000 Y4.697 F4800.000 ; move to first external small perimeter point
G1 F600.000
G1 X-4.781 Y-4.865 E0.08698 ; external small perimeter
G1 X4.781 Y-4.865 E0.07780 ; external small perimeter
G1 X0.028 Y4.642 E0.08648 ; external small perimeter
G1 Z0.681 F4800.000 ; move to next layer (1)
;BIOX_ALTERNATING_PERIMETER_LAYER_1
G1 X0.000 Y4.496 F4800.000 ; move to first external small perimeter point
G1 F600.000
G1 X-4.635 Y-4.774 E0.21823 ; external small perimeter
G1 X4.635 Y-4.774 E0.19519 ; external small perimeter
G1 X0.028 Y4.441 E0.21694 ; external small perimeter END
G1 Z30000.271 F4800.000 ; lift printhead 3 cm

; Filament-specific end gcode
;END gcode for filament

M104 S0 ; turn off temperature
G28 X0  ; home X axis
M84     ; disable motors

M140 S0 ; set bed temperature
```

```
; filament used = 3.1mm (0.0cm3)
; total filament cost = 0.0
```

A.2 Words AIMES and RAYS

```
; Print Config Notes:
; This profile prints tissue model with upright square lattice structure.
;
; external perimeters extrusion width = 0.45mm (1.49mm^3/s)
; perimeters extrusion width = 0.43mm (1.40mm^3/s)
; infill extrusion width = 0.43mm (1.40mm^3/s)
; solid infill extrusion width = 0.43mm (1.40mm^3/s)
; top infill extrusion width = 0.43mm (1.40mm^3/s)



M104 S200 ; set temperature
G28 ; home all axes
G1 Z5 F5000 ; lift nozzle

G1 Z0.671 F4800.000 ; put back nozzle layer (1)
G1 Z0.271 F4800.000 ; put back nozzle layer (0)

; Filament gcode
; AIMES

M109 S200 ; set temperature and wait for it to be reached
G21 ; set units to millimeters
G90 ; use absolute coordinates
```

```
M83 ; use relative distances for extrusion
G1 Z0.271 F4800.000 ; move to next layer (0)
;BIOX_ALTERNATING_PERIMETER_LAYER_0



; letter A
G1 X-32.5 Y10 F4800.000 ; move to first external small perimeter point
G1 F600.000
G1 Z0.271 F4800.000 ; put back nozzle layer (0)
G1 F600.000
G1 X-27.5 Y20 E0.00389 ; external small perimeter
G1 X-22.5 Y10 E0.00389 ; external small perimeter
G1 Z5 F5000 ; lift nozzle
G1 X-30 Y15 ; external small perimeter
G1 Z0.271 F4800.000 ; put back nozzle layer (0)
G1 F600.000
G1 X-25 Y15 E0.00389 ; external small perimeter
G1 Z5 F5000 ; lift nozzle
G1 X-32.5 Y10 F4800.000 ; move to first external small perimeter point
G1 Z0.671 F4800.000 ; move to next layer (1)
G1 F600.000
G1 X-27.5 Y20 E0.00389 ; external small perimeter
G1 X-22.5 Y10 E0.00389 ; external small perimeter
G1 Z5 F5000 ; lift nozzle
G1 X-30 Y15 ; external small perimeter
G1 Z0.671 F4800.000 ; put back nozzle layer (1)
G1 F600.000
G1 X-25 Y15 E0.00389 ; external small perimeter
```

```
; letter I
G1 Z5 F5000 ; lift nozzle
G1 X-20 Y10 F4800.000 ; external small perimeter
G1 Z0.271 F4800.000 ; move to next layer (0)
G1 F600.000
G1 X-10 Y10 E0.00389; external small perimeter'
G1 Z5 F5000 ; lift nozzle
G1 X-15 Y10 ; external small perimeter
G1 Z0.271 F4800.000 ; put back nozzle layer (0)
G1 F600.000
G1 X-15 Y20 E0.00389; external small perimeter
G1 Z5 F5000 ; lift nozzle
G1 X-20 Y20 ; external small perimeter
G1 Z0.271 F4800.000 ; put back nozzle layer (0)
G1 F600.000
G1 X-10 Y20 E0.00389; external small perimeter
G1 Z5 F5000 ; lift nozzle
G1 X-20 Y10 F4800.000 ; external small perimeter
G1 Z0.671 F4800.000 ; move to next layer (1)
G1 F600.000
G1 X-10 Y10 E0.00389; external small perimeter
G1 Z5 F5000 ; lift nozzle
G1 X-15 Y10 ; external small perimeter
G1 Z0.671 F4800.000 ; put back nozzle layer (1)
G1 F600.000
G1 X-15 Y20 E0.00389; external small perimeter
```

```
G1 Z5 F5000 ; lift nozzle
G1 X-20 Y20 ; external small perimeter
G1 Z0.671 F4800.000 ; put back nozzle layer (1)
G1 F600.000
G1 X-10 Y20 E0.00389; external small perimeter


; letter M
G1 Z5 F5000 ; lift nozzle
G1 X-5 Y10 F4800.000 ; external small perimeter ; external small perimeter
G1 Z0.271 F4800.000 ; move to next layer (0)
G1 F600.000
G1 X-5 Y20 E0.00389; external small perimeter
G1 X0 Y15 E0.00389; external small perimeter
G1 X5 Y20 E0.00389; external small perimeter
G1 X5 Y10 E0.00389; external small perimeter
G1 Z5 F5000 ; lift nozzle
G1 X-5 Y10 F4800.000 ; external small perimeter ; external small perimeter
G1 Z0.671 F4800.000 ; move to next layer (1)
G1 F600.000
G1 X-5 Y20 E0.00389; external small perimeter
G1 X0 Y15 E0.00389; external small perimeter
G1 X5 Y20 E0.00389; external small perimeter
G1 X5 Y10 E0.00389; external small perimeter

; letter E
G1 Z5 F5000 ; lift nozzle
G1 X20 Y10 F4800.000 ; external small perimeter
```

```
G1 Z0.271 F4800.000 ; move to next layer (0)
G1 F600.000
G1 X10 Y10 E0.00389 ; external small perimeter
G1 X10 Y20 E0.00389 ; external small perimeter
G1 X20 Y20 E0.00389 ; external small perimeter
G1 Z5 F5000 ; lift nozzle
G1 X15 Y15 F4800.000 ; external small perimeter
G1 Z0.271 F4800.000 ; put back nozzle layer (0)
G1 F600.000
G1 X10 Y15 E0.00389 ; external small perimeter
G1 Z5 F5000 ; lift nozzle
G1 X20 Y10 F4800.000 ; external small perimeter
G1 Z0.671 F4800.000 ; move to next layer (1)
G1 F600.000
G1 X10 Y10 E0.00389 ; external small perimeter
G1 X10 Y20 E0.00389 ; external small perimeter
G1 X20 Y20 E0.00389 ; external small perimeter
G1 Z5 F5000 ; lift nozzle
G1 X15 Y15 F4800.000 ; external small perimeter
G1 Z0.671 F4800.000 ; put back nozzle layer (1)
G1 F600.000
G1 X10 Y15 E0.00389 ; external small perimeter


; letter S
G1 Z5 F5000 ; lift nozzle
G1 X22.5 Y10 F4800.000 ; external small perimeter
G1 Z0.271 F4800.000 ; move to next layer (0)
```

```
G1 F600.000
G1 X29.5 Y10 E0.00389 ; external small perimeter
G1 X31.5 Y11 E0.00389 ; external small perimeter
G1 X32.5 Y12 E0.00389 ; external small perimeter
G1 X32.5 Y13 E0.00388 ; external small perimeter
G1 X31.5 Y14 E0.00388 ; external small perimeter
G1 X29.5 Y15 E0.00389 ; external small perimeter
G1 X25.5 Y15 E0.00389 ; external small perimeter
G1 X23.5 Y16 E0.00389 ; external small perimeter
G1 X22.5 Y17 E0.00388 ; external small perimeter
G1 X22.5 Y18 E0.00388 ; external small perimeter
G1 X23.5 Y19 E0.00389 ; external small perimeter
G1 X25.5 Y20 E0.00389 ; external small perimeter
G1 X32.5 Y20 E0.00389 ; external small perimeter
G1 Z5 F5000 ; lift nozzle
G1 X22.5 Y10 F4800.000 ; external small perimeter
G1 Z0.671 F4800.000 ; move to next layer (1)
G1 F600.000
G1 X29.5 Y10 E0.00389 ; external small perimeter
G1 X31.5 Y11 E0.00389 ; external small perimeter
G1 X32.5 Y12 E0.00389 ; external small perimeter
G1 X32.5 Y13 E0.00388 ; external small perimeter
G1 X31.5 Y14 E0.00388 ; external small perimeter
G1 X29.5 Y15 E0.00389 ; external small perimeter
G1 X25.5 Y15 E0.00389 ; external small perimeter
G1 X23.5 Y16 E0.00389 ; external small perimeter
G1 X22.5 Y17 E0.00388 ; external small perimeter
G1 X22.5 Y18 E0.00388 ; external small perimeter
```

```
G1 X23.5 Y19 E0.00389 ; external small perimeter
G1 X25.5 Y20 E0.00389 ; external small perimeter
G1 X32.5 Y20 E0.00389 ; external small perimeter


; letter R
G1 Z5 F5000 ; lift nozzle
G1 X-15 Y-15 F4800.000 ; move to first external small perimeter point
G1 Z0.271 F4800.000 ; move to next layer (0)
G1 F600.000
G1 X-15 Y-5 E0.00389 ; external small perimeter
G1 X-13 Y-5 E0.00389 ; external small perimeter
G1 X-11 Y-6 E0.00389 ; external small perimeter
G1 X-10 Y-7 E0.00389 ; external small perimeter
G1 X-10 Y-8 E0.00389 ; external small perimeter
G1 X-11 Y-9 E0.00389 ; external small perimeter
G1 X-13 Y-10 E0.00389 ; external small perimeter
G1 X-15 Y-10 E0.00389 ; external small perimeter
G1 X-10 Y-15 E0.00389 ; external small perimeter
G1 Z5 F5000 ; lift nozzle
G1 X-15 Y-15 F4800.000 ; move to first external small perimeter point
G1 Z0.671 F4800.000 ; move to next layer (1)
G1 F600.000
G1 X-15 Y-5 E0.00389 ; external small perimeter
G1 X-13 Y-5 E0.00389 ; external small perimeter
G1 X-11 Y-6 E0.00389 ; external small perimeter
G1 X-10 Y-7 E0.00389 ; external small perimeter
G1 X-10 Y-8 E0.00389 ; external small perimeter
```

```
G1 X-11 Y-9 E0.00389 ; external small perimeter
G1 X-13 Y-10 E0.00389 ; external small perimeter
G1 X-15 Y-10 E0.00389 ; external small perimeter
G1 X-10 Y-15 E0.00389 ; external small perimeter


; letter A
G1 Z5 F5000 ; lift nozzle
G1 X-5 Y-15 F4800.000 ; move to first external small perimeter point
G1 Z0.271 F4800.000 ; move to next layer (0)
G1 F600.000
G1 X-2.5 Y-5 E0.00389 ; external small perimeter
G1 X0 Y-15 E0.00389 ; external small perimeter
G1 Z5 F5000 ; lift nozzle
G1 X-4 Y-10 F4800.000 ; move to first external small perimeter point
G1 Z0.271 F4800.000 ; put back nozzle layer (0)
G1 F600.000
G1 X-1 Y-10 E0.00389 ; external small perimeter
G1 Z5 F5000 ; lift nozzle
G1 X-5 Y-15 F4800.000 ; move to first external small perimeter point
G1 Z0.671 F4800.000 ; move to next layer (1)
G1 F600.000
G1 X-2.5 Y-5 E0.00389 ; external small perimeter
G1 X0 Y-15 E0.00389 ; external small perimeter
G1 Z5 F5000 ; lift nozzle
G1 X-4 Y-10 F4800.000 ; move to first external small perimeter point
G1 Z0.671 F4800.000 ; put back nozzle layer (1)
G1 F600.000
```

```
G1 X-1 Y-10 E0.00389 ; external small perimeter

; letter Y
G1 Z5 F5000 ; lift nozzle
G1 X5 Y-5 F4800.000 ; move to first external small perimeter point
G1 Z0.271 F4800.000 ; move to next layer (0)
G1 F600.000
G1 X7.5 Y-10 E0.00389 ; external small perimeter
G1 Z5 F5000 ; lift nozzle
G1 X10 Y-5 F4800.000 ; move to first external small perimeter point
G1 Z0.271 F4800.000 ; put back nozzle layer (0)
G1 F600.000
G1 X5 Y-15 E0.00389 ; external small perimeter
G1 Z5 F5000 ; lift nozzle
G1 X5 Y-5 F4800.000 ; move to first external small perimeter point
G1 Z0.671 F4800.000 ; move to next layer (1)
G1 F600.000
G1 X7.5 Y-10 E0.00389 ; external small perimeter
G1 Z5 F5000 ; lift nozzle
G1 X10 Y-5 F4800.000 ; move to first external small perimeter point
G1 Z0.671 F4800.000 ; put back nozzle layer (1)
G1 F600.000
G1 X5 Y-15 E0.00389 ; external small perimeter

; letter S
G1 Z5 F5000 ; lift nozzle
G1 X15 Y-15 F4800.000 ; move to first external small perimeter point
G1 Z0.271 F4800.000 ; move to next layer (0)
```

```
G1 F600.000
G1 X17.5 Y-15 E0.00389 ; external small perimeter
G1 X19 Y-14 E0.00389 ; external small perimeter
G1 X20 Y-13 E0.00389 ; external small perimeter
G1 X20 Y-12 E0.00389 ; external small perimeter
G1 X19 Y-11 E0.00389 ; external small perimeter
G1 X17.5 Y-10 E0.00389 ; external small perimeter
G1 X16 Y-9 E0.00389 ; external small perimeter
G1 X15 Y-8 E0.00389 ; external small perimeter
G1 X15 Y-7 E0.00389 ; external small perimeter
G1 X16 Y-6 E0.00389 ; external small perimeter
G1 X17.5 Y-5 E0.00389 ; external small perimeter
G1 X20 Y-5 E0.00389 ; external small perimeter
G1 Z5 F5000 ; lift nozzle
G1 X15 Y-15 F4800.000 ; move to first external small perimeter point
G1 Z0.671 F4800.000 ; move to next layer (1)
G1 F600.000
G1 X17.5 Y-15 E0.00389 ; external small perimeter
G1 X19 Y-14 E0.00389 ; external small perimeter
G1 X20 Y-13 E0.00389 ; external small perimeter
G1 X20 Y-12 E0.00389 ; external small perimeter
G1 X19 Y-11 E0.00389 ; external small perimeter
G1 X17.5 Y-10 E0.00389 ; external small perimeter
G1 X16 Y-9 E0.00389 ; external small perimeter
G1 X15 Y-8 E0.00389 ; external small perimeter
G1 X15 Y-7 E0.00389 ; external small perimeter
G1 X16 Y-6 E0.00389 ; external small perimeter
G1 X17.5 Y-5 E0.00389 ; external small perimeter
```

```
G1 X20 Y-5 E0.00389 ; external small perimeter

; Filament-specific end gcode
;END gcode for filament

M104 S0 ; turn off temperature
G28 X0  ; home X axis
M84     ; disable motors

M140 S0 ; set bed temperature

; filament used = 0.9mm (0.0cm3)
; total filament cost = 0.0
```